J. Biochem. **143,** 69–78 (2008)
doi:10.1093/jb/mvm193

Structural Basis for the Decarboxylation of Orotidine 5′-Monophosphate (OMP) by *Plasmodium Falciparum* OMP Decarboxylase†

Keiji Tokuoka[1], Yukiko Kusakari[1], Sudaratana R. Krungkrai[2,3], Hiroyoshi Matsumura[1], Yasushi Kai[1], Jerapan Krungkrai[4], Toshihiro Horii[2] and Tsuyoshi Inoue[1,*]

[1]Department of Applied Chemistry, Graduate School of Engineering, Osaka University, 2-1 Yamadaoka, Suita, Osaka 565-0871; [2]Department of Molecular Protozoology, Research Institute for Microbial Diseases, Osaka University, 3-1 Yamadaoka, Suita, Osaka 565-0871, Japan; [3]Unit of Biochemistry, Department of Medical Science, Faculty of Science, Rangsit University, Patumthani 12000; and [4]Department of Biochemistry, Faculty of Medicine, Chulalongkorn University, Rama IV Road, Bangkok 10330, Thailand

Received August 6, 2007; accepted October 2, 2007; published online November 1, 2007

Orotidine 5′-monophoshate decarboxylase (OMPDC) catalyses the decarboxylation of orotidine 5′-monophosphate (OMP) to uridine 5′-monophosphate (UMP). Here, we report the X-ray analysis of apo, substrate or product-complex forms of OMPDC from *Plasmodium falciparum* (*Pf*OMPDC) at 2.7, 2.65 and 2.65 Å, respectively. The structural analysis provides the substrate recognition mechanism with dynamic structural changes, as well as the rearrangement of the hydrogen bond array at the active site. The structural basis of substrate or product binding to *Pf*OMPDC will help to uncover the decarboxylation mechanism and facilitate structure-based optimization of antimalarial drugs.

Key words: apo form, OMP-complex, orotidine 5′-monophoshate decarboxylase, structural comparison, UMP-complex, x-ray structural analysis.

Abbreviations: OMP, orotidine 5′-monophosphate; OMPDC, OMP decarboxylase; PfOMPDC, OMPDC from *Plasmodium falciparum*; OPRT, orotate phosphoribosyltransferase; SDS–PAGE, sodium dodecyl sulfate–polyacrylamide gel electrophoresis.

Human malaria is caused by four species of the parasitic protozoan genus *Plasmodium*. Of these four species, *Plasmodium falciparum* is responsible for the vast majority of the 500 million episodes of malaria worldwide, and accounts for 2–3 million deaths annually (*1*). Chemotherapy of malaria is available, but is complicated by drug toxicity and widespread resistance to most of the currently available antimalarial drugs (*2*). There is an urgent need for more efficacious and less-toxic agents, particularly rational drugs that exploit pathways and targets unique to the parasite. In general, drug-screening procedures have rarely been applied to this disease, and there is a paucity of information on a number of biochemical pathways that can be exploited for chemotheraphy. The malarial parasite is totally dependent on *de novo* pyrimidine biosynthesis for its growth and development because it lacks the relevant salvage enzymes (*3–5*). The *de novo* pathway contains six reaction steps. The initial reaction catalysed by carbamoyl phosphate synthetase is the formation of carbamoyl phosphate by combination of carbonate, ATP and an amino group from glutamine. Three additional reactions are necessary to form the pyrimidine ring from carbamoyl phosphate. In the final two steps, uridine 5′-monophosphate (UMP) requires the addition of a ribose phosphate moiety from 5-phosphoribosyl-1-pyrophosphate to orotate by orotate phosphoribosyltransferase (EC 2.4.2.10, OPRT) to form orotidine 5′-monophosphate (OMP) and pyrophosphate (PP_i), and the subsequently decarboxylation of OMP to form UMP, by OMP decarboxylase (EC 4.1.1.23, OMPDC).

In most prokaryotes and yeasts (*6*, *7*), the OPRT and OMPDC enzymes are encoded by two separate genes, while in most multicellular eukaryotes, the genes for both enzymes have been joined into a single gene, resulting in the expression of a bifunctional protein, namely UMP synthase, with two different catalytic domains (*8–11*). The bifunctional UMP synthase has also been reported in kinetoplastid parasites, e.g. *Trypanosoma cruzi* and *Leishmania mexicana* (*12*, *13*). In contrast, mammalian hosts can utilize both the *de novo* and salvage pathways (*8*, *14*). Inhibitors of the *de novo* pathway have strong antimalarial activity for *in vitro P. falciparum* growth (*15–18*).

The sequence alignment for 10 known crystal structures of OMPDC is shown in Fig. 1. This reveals the existence of 11 totally conserved amino acid residues (shaded in red), corresponding to Asp23, Lys102, Asp136, Lys138, Asp141, Ile142, Gly169, Pro264, Gly265, Gly293 and Arg294 in *P. falciparum*. The alanine replacement around the active site, however, shows that *Plasmodium* OMPDCs have somewhat different sequences (*19*). The most striking observation is that a large insertion

*To whom correspondence should be addressed. Tel: +81-6-6879-7410, Fax: +81-6-6879-7409,
E-mail: inouet@chem.eng.osaka-u.ac.jp
†Coordinates have been deposited in the Protein Data Bank (accession codes 2ZA2, 2ZA1 and 2ZA3 for the apo form, and OMP- or UMP-complex of PfOMPDC, respectively).

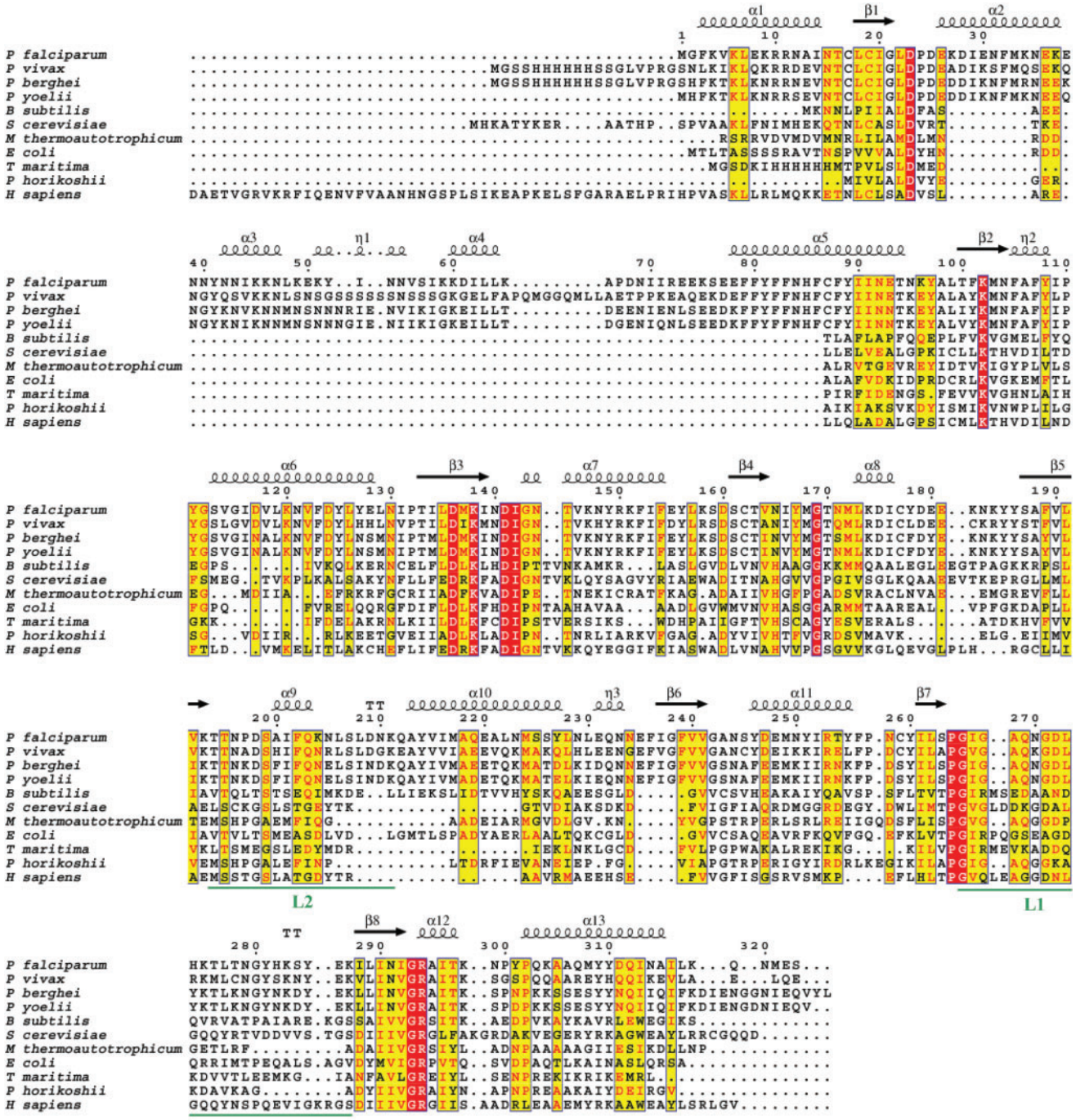

Fig. 1. **Multiple sequence alignments of *Pf*OMPDC compared with those of 10 known crystal structures.** PDB IDs are showed in parentheses: *Plasmodium vivax* (2FFC) (*48*), *Plasmodium berghei* (2FDS) (*48*), *Plasmodium yoelii* (2AQW) (*48*), *Bacillus subtilis* (1DBT) (*24*), *Saccharomyces cerevisiae* (1DQW) (*32*), *M. thermoautotrophicum* (1DV7) (*22*), *E. coli* (1L2U) (*49*), *Thermotoga maritima* (1VQT), *Pyrococcus horikoshii* (2CDZ) and *Homo sapiens* (2EAW). Red-shaded amino acids are conserved in all 10 sequences; yellow-shaded amino acids are similar residues. Above the sequences, the secondary structural elements are shown, as identified in *Pf*OMPDC. The L1 and L2 loops are identified and marked by bottom underlines.

is present at the N-terminal domain, in all *Plasmodium* OMPDCs. It has been proposed that the N-terminal domain of *Pf*OMPDC binds to that of *P. falciparum* OPRT (*Pf*OPRT) (*20*).

Currently, the most accredited mechanisms involve direct decarboxylation of OMP (*21*). This was proposed based on X-ray analysis of the structure of OMPDC–inhibitor complexes (*22–28*), and is supported by a wealth of theoretical and experimental studies (*22*, *29–31*). It has been proposed that the protonation/decarboxylation of OMP could be a concerted event at the direct decarboxylation (*23*). In contrast, some other experimental

evidence supports the formation of a carboanionic intermediate upon decarboxylation (*32*, *33*). In both cases, kinetic studies have unambiguously identified Lys72 (*Methanobacterium thermoautotrophicum* numbering) as the residue that protonates the C6 center (*21*, *34*, *35*). Another recently proposed catalytic mechanism assumes a preliminary protonation of the uracil ring far from the decarboxylation center. Kollman (*36*), assuming a protonated Asp70, has proposed as a first step in decarboxylation, an interesting mechanism involving an enamine protonation at C5 carried out by the Lys72 residue (*M. thermoautotrophicum* numbering). Furthermore, based on *ab initio* calculations, it has been proposed that O2 and O4 are protonated prior to decarboxylation (*36*, *37*). The latest proposals for this reaction mechanism strongly support direct decarboxylation of OMP, with the formation of a carboanionic intermediate via a transition-state stabilization mechanism, in which the fully conserved Lys72 (*M. thermoautotrophicum* numbering) plays a fundamental role by stabilizing the forming negative charge at C6, and consequently, the transition state (*31*).

In this study, we report the X-ray analysis of the apo, substrate- and product-complex forms of OMPDC from *P. falciparum* (*Pf*OMPDC). This structural analysis provides us with a substrate recognition mechanism with dynamic structural changes, as well as the rearrangement of the hydrogen-bond array occurring during enzymatic catalysis at the active site. We also propose a protruding domain at the N-terminal insertion of *Pf*OMPDC is responsible for binding to *Pf*OPRT.

MATERIALS AND METHODS

Protein Expression and Purification—The recombinant OMPDC protein was prepared by cloning and expression of the gene encoding *Pf*OMPDC in *Escherichia coli*. The oligonucleotide primers were 5′-CG**G GAT CC**A TGG GTT TTA AGG TAA AAT TA-3′ and 5′-CC**A TCG AT**T TAC GAT TCC ATA TTT TGC TTT AA-3′, which includes encompass *BamH*I and *Cla*I restriction sites (in bold), respectively. Polymerase chain reaction (PCR) was carried out using *Pfu* DNA polymerase (Promega) at 95°C for 5 min, followed by 40 cycles of 95°C for 1 min, 55°C for 1 min and 68°C for 3 min, with a final 68°C for 10 min. The expected 980 bp product for full-length *Pf*OMPDC was inserted into the linearized expression vector pTrcHis-TOPO (Invitrogen). *Escherichia coli* TOP10 (Invitrogen) cells were transformed with the recombinant plasmid and induced with 1 mM isopropyl β-D-thiogalactopyranoside at 37°C for 18–20 h, and the cell paste was harvested by centrifugation at 8000*g* for 10 min. The recombinant enzyme was expressed as a soluble protein, and further purified by using a Ni^{2+}-nitrilotriacetic acid-agarose affinity column (Qiagen) with 50 mM Tris–HCl, pH 8.0, 300 mM NaCl, 250 mM imidazole and 10% glycerol as the eluting buffer. Further purification was achieved using a Superdex-75 Hiload 26/60 column (GE Healthcare) on ÄKTA fast protein liquid chromatography (GE Healthcare) equilibrated with 50 mM Tris–HCl, pH 8.0, 300 mM NaCl, 5 mM dithiothreitol. The enzyme activity was eluted as a single symmetrical peak at a position of 76 kDa. SDS–PAGE analysis (*38*) showed that the homogeneous preparation had a molecular mass of 38 kDa. The active form of *Pf*OMPDC was a dimer. OMPDC activity was monitored by a decrease in absorbance of OMP at 285 nm, as described previously (*11*). The purified recombinant enzyme had a specific activity of $\sim$10 μmol min^{-1} (mg protein)$^{-1}$, 300-fold purification, and 30% yield. Up to 30 mg pure recombinant protein was obtained from 10 L of the *E. coli* cell culture. The purified protein was concentrated by Centricon ultrafiltration to 10 mg mL^{-1}, and the homogeneity was confirmed by dynamic light scattering with DynaPro-MS/X (Protein Solutions).

Data Collection and Processing—The apo form was crystallized by a previously reported method (*39*). Complex crystals with OMP or UMP were prepared by soaking in a solution containing 10 mM OMP or UMP for 2 min.

X-ray diffraction data from the apo form were collected at X06SA beamline (Swiss Light Source, Switzerland) and from OMP- or UMP-complex at BL38 beamline (SPring-8, Japan). Prior to data collection, crystals of apo form and OMP- or UMP-complex of *Pf*OMPDC were soaked in a cryoprotectant solution consisting of 23% (w/v) PEG3K, 0.1 M CHES (pH 9.5) and 8% glycerol. The apo form and OMP- or UMP-complex were then mounted in a standard nylon loop in a stream of liquid nitrogen at 100 K. The diffraction patterns were recorded on a MarCCD detector (Mar Research) for the apo form, and on an ADSC Quantum detector (Area Detector Systems Corporation) for the complexes at cryogenic temperature (100 K).

The diffraction intensity data were processed and scaled using MOSFLM (*40*) and HKL2000 (*41*). The statistics of the diffraction data collection are shown in Table 1.

Structure Determination and Refinement—The molecular replacement calculations were performed with the program MOLREP (*42*) in the CCP4 program package (*43*), using the PO_4-complex of *Pf*OMPDC (PDB code: 2f84) as the search model. A dimer molecule was located in an asymmetric unit of the crystal. Structure models of the apo form were refined against the diffraction data using CNS (*44*) and REFMAC (*45*). The models were manually adjusted by electron density map using COOT (*46*). Even after several cycles of refinement, the electron density for residues 70–74 and 268–274 for one subunit, and 68–70 and 268–272 for the other subunit, was poor. Some other parts of the side chain structure (residues 1, 35, 69, 75, 76, 79, 199, 201, 255, 269, 275, 281, 301, 306, 314, 317 and 318 for one subunit; and residues 1, 71, 96, 174, 207, 222, 231, 255, 266, 269, 273, 274, 275, 281, 306, 314, 317 and 318 for the other subunit) also had poor electron density. The models for these residues were built by using alanine. All models were refined for a few cycles of CNS with B-factor refinement until convergence. The coordinates of the apo, and OMP- or UMP-complex forms of *Pf*OMPDC was deposited as 2ZA2, 2ZA1 and 2ZA3 in the Protein Data Bank. Final refinement statistics for the refined coordinate sets for three structures are shown in Table 1.

Table 1. **Data collection and refinement statistics.**

	apo form	OMP-complex	UMP-complex
Diffraction data			
Space group cell dimensions (Å)	*R3*	*R3*	*R3*
a	201.81	201.87	202.49
b	201.81	201.87	202.49
c	44.03	44.19	44.36
Resolution (Å)	50.0–2.70 (2.85–2.70)	50.0–2.60 (2.69–2.60)	50.0–2.60 (2.69–2.60)
Measured reflections (n)	57,278	105,551	65,099
Unique reflections (n)	18,313	20,677	20,877
Completeness (%)	99.6 (100.0)	98.8 (99.2)	99.0 (99.9)
R^{a}_{merge} (%)	5.9 (27.5)	8.6 (33.9)	8.7 (31.7)
Refinement statistics			
Resolution (Å)	50–2.70	50–2.65	50–2.65
R^{b}_{cryst} (%)	21.6	20.8	21.1
R^{c}_{free} (%)	31.2	28.3	29.4
No. of water molecules	39	134	56
Root mean square deviation bond length (Å)	0.007	0.009	0.007
Root mean square deviation bond angle (°)	1.4	1.9	1.4

[a] $R_{merge} = \sum|I(k) - I|/\sum I(k)$, where $I(k)$ is value of the kth measurement of the intensity of a reflection, I is the mean value of the intensity of that reflection and the summation is the over all measurements. [b] $R_{cryst} = \sum||F_o| - |F_c||/\sum|F_o|$ calculated from 90% of the data, which were used during the course of the refinement. [c] $R_{free} = \sum||F_o| - |F_c||/\sum|F_o|$ calculated from 10% of the data, which were used during the course of the refinement.

RESULTS

Overall Structure—The 2.7 Å structure of the apo form of *Pf*OMPDC was solved with R and R_{free} values of 21.6 and 31.2, respectively, by using the MR method with the PO_4-complex of *Pf*OMPDC. *Pf*OMPDC was crystallized in the trigonal space group of *R*3. One dimer molecule existed in the asymmetric unit (Fig. 2a). The dimer interface was consisted of 10 hydrogen-bond interactions, Lys138(A)-Asp141(B), Asn140(A)-Asn165(B), Asn140(A)-Lys138(B), Asp141(A)-Lys138(B), Lys151(A)-Glu26(B), Asn165(A)-Asn140(B), Asn165(A)-Asn165(B), Asn196(A)-Met168(B), Asp198(A)-Asn171(B) and Asp198(A)-Thr170(B) (Fig. 2b). Each OMPDC subunit of this dimeric enzyme folded as an $(\alpha/\beta)_8$ barrel, with eight central β-sheets surrounded by 13 α helices (Fig. 2c). β1, residues 18–21; β2, 100–104; β3, 132–139; β4, 161–164; β5, 187–193; β6, 237–241; β7, 261–263; and β8, 288–292; and α1, residues 3–14; α2, 26–37; α3, 42–47; α4, 60–64; α5, 78–94; α6, 113–128; α7, 143–154; α8, 173–176; α9, 200–203; α10, 213–227; α11, 246–255; α12, 276–279 and α13, 302–315. There were three extra short α helices: η1, residues 51–54; η2, 105–108 and η3, 230–233 (Fig. 2d).

As predicted from protein sequence analysis (Fig. 1), there was a large insertion region (*48–86*), forming α3, η1 and α4 helices and extended α5-helix (Fig. 2b). Also *Pf*OMPDC contained a small insertion region (208–217), extended α10 helix. These insertions are not found in other characterized OMPDC structures outside of the *Plasmodium* species, and appear to be a unique structural feature of the *Plasmodium* OMPDCs.

The active site was located at the open end of the $(\alpha/\beta)_8$ barrel, which corresponded to the carboxy-terminal of the β strands and the amino-terminal of the α helices. In the apo structure, the L1 loop comprised of residues 268–274 was disordered around the active site, while the L1 loop structure was stabilized upon binding of substrate or product. The detailed structural comparison between the apo and holo form is described later.

Structural Changes of L1 and L2 Loops upon Binding of OMP/UMP—The structural analysis of *Pf*OMPDC complexes has been performed with R and R_{free} values of 20.8 and 28.3, respectively for the 2.65 Å structure complexed with OMP, and 21.1 and 29.4, respectively, for the 2.65 Å with UMP.

Comparison between the apo and OMP- or UMP-complex of *Pf*OMPDC showed a root-mean-square deviation of 0.75 and 0.74 Å, respectively, by using for 318 structurally equivalent C_α atom positions. Several notable structural differences were found around the active site near the open end of the $(\alpha/\beta)_8$ barrel upon binding of OMP or UMP.

The L1 loop which was not determined in the apo form, was stabilized upon binding of the ligands, preventing from solvent. Glu269 in the L1 loop access to the pyrimidine ring moiety of OMP or UMP formed the loop structure of L1 (Fig. 3a). While the structure of the α9 helix was formed in the L2 loop region (194–213) in the apo form, the secondary structure unfolded in the presence of OMP or UMP, associated with the movement of Thr195 (Fig. 3b). The difference in C_α position and the dihedral bond angle of C_β–C_γ in Thr195 was calculated to be 3.8 Å and 149.1°, respectively, between the apo and OMP-complex; and 3.6 Å and 150.0°, respectively, between the apo and UMP-complex. It was revealed that both the L1 and L2 loops recognized the pyrimidine ring with the large structural changes. The details of the structural changes to the active site of *Pf*OMPDC are described later.

Change in Active-Site Structure upon Binding of OMP/UMP—Schematic drawings of the OMP- or UMP-complex are shown in Fig. 4a and b, respectively. Both the guanidium group and the backbone amide of Arg294 interacted directly with the phosphate group of OMP

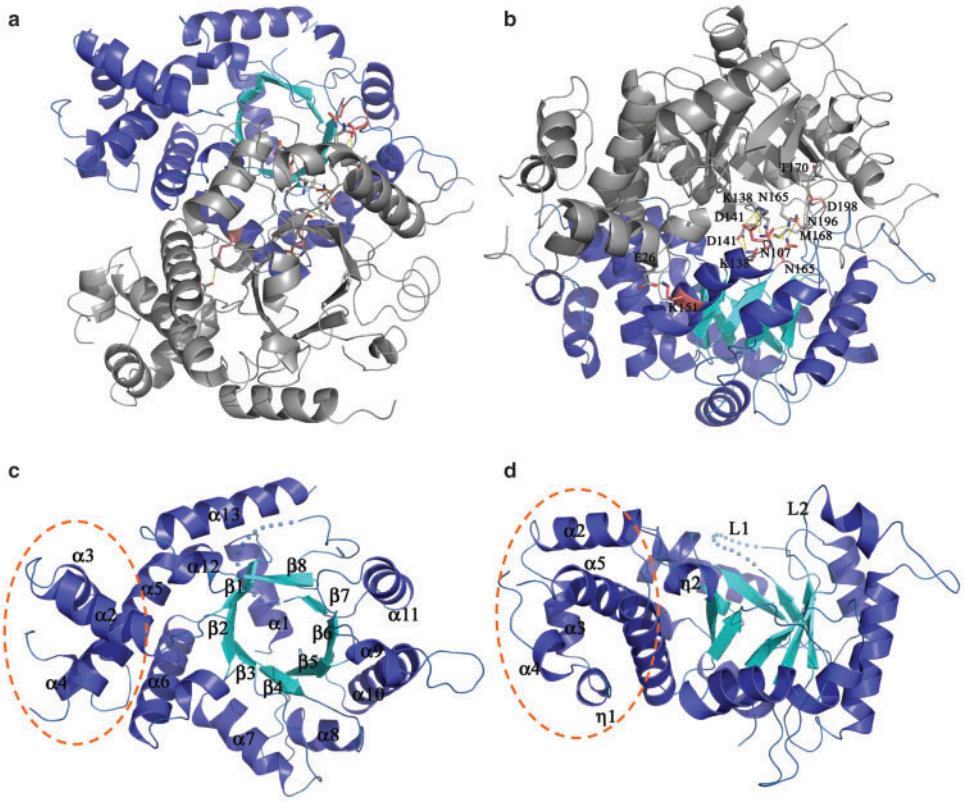

Fig. 2. **Mol-A (colour in blue) and mol-B (colour in gray) forms a dimer structure of *Pf*OMPDC.** (a) Viewed through α/β barrel. (b) Viewed perpendicular to the view in panel 2a. Monomer of *Pf*OMPDC. The α helices (in blue) and β sheets (in cyan) are separated by loops. One subunit folds as an $(\alpha/\beta)_8$ barrel with eight central β sheets surrounded by 13 α helices. The disordered L1 loop is shown as a dotted line. (c) Viewed from same direction as the mol-A in 2a. (d) Viewed from same direction as the mol-A in 2b. A large insertion region from residue 48 to 86, constructed the insertion domain containing three helices, and was presented in dot circle (in orange). The figures were drawn with PYMOL (*50*).

or UMP, as did the amide of Gly293. Thr145(B) and Asn104 hydrogen-bonded to the 2′- and 3′-hydroxyl group of the ribose ring, respectively. In the top part of the pyrimidine ring, comprising O4, N3 and O2, there were hydrogen bonds to Thr195 and Gln269. Thr195 accepted a hydrogen bond from N3 and donated a hydrogen bond to O4. A pocket near C5 of the pyrimidine ring was surrounded by several hydrophobic residues of Ile142(B), Leu191, Thr194, Val240 and Pro264 (not shown in Fig. 4a).

Compared with the apo form, there was a change in active-site structure upon ligand binding. Arg294 and Thr195 in L2, and Gln269 in L1 exhibited a large structural movement upon binding of OMP or UMP. The averaged movement of three nitrogen positions in the guanidium residue of Arg294 were both calculated to be 2.9 Å for the OMP- or UMP-complexes, and the dihedral angles of C_δ–N_ε and N_ε–C_ζ of Arg294 are 120.1° and 87.2° for OMP-, and 64.6° and 118.2° for UMP-complexes, respectively. The helix structure of α12 did not change, while the L1 and L2 loops had the large structural movements described earlier. The average difference in the top part of residues Thr195 and Arg294 was measured to be 1.5 and 1.6 Å, respectively for OMP- and UMP-complexes. On the other hand, in the bottom part of the active site, the C_α atom of Gln293, Asn104 and Thr145(B) adopted almost the same positions between the apo and complex forms. The average difference in the bottom part of residues Asn104, Thr145(B) and Gln293 was 0.3 Å for both the OMP- and UMP-complexes.

The binding mode of OMP was basically the same as that of UMP, except for the residue Lys102. In the OMP binding form, Lys102 hydrogen-bonded to the carboxylate oxygen of pyrimidine. After decarboxylation, Lys102 changed the hydrogen bond to O5 of ribose (Fig. 4).

Rearrangement of Hydrogen-Bond Network Around Lys102—In the apo form, Lys102 formed a hydrogen-bond network with Asp136, Lys138 and Asp141 from the other protomer of the dimer (Fig. 5a). The conserved catalytic array of Lys102-Asp136-Lys138-Asp141(B) makes the hydrogen-bond network at the active site. The amino group of Lys102 recognized the carboxyl group of OMP, and then the distance between Lys102-Asp136 was lengthened from 2.7 to 3.6 Å, breaking the hydrogen bond between Lys102 and Asp136 upon binding of OMP (Fig. 5b and d). The UMP binding form (Fig. 5c and e), which mimicked the structure after decarboxylation, possessed two hydrogen bonds at Lys102-Asp136 and Lys138-Asp141(B) (Fig. 5c). In the UMP-complex, Lys102 hydrogen bonded to Asp136 instead of the carboxyl group of the pyrimidine ring, breaking the hydrogen bond between Asp136 and Lys138, after decarboxylation.

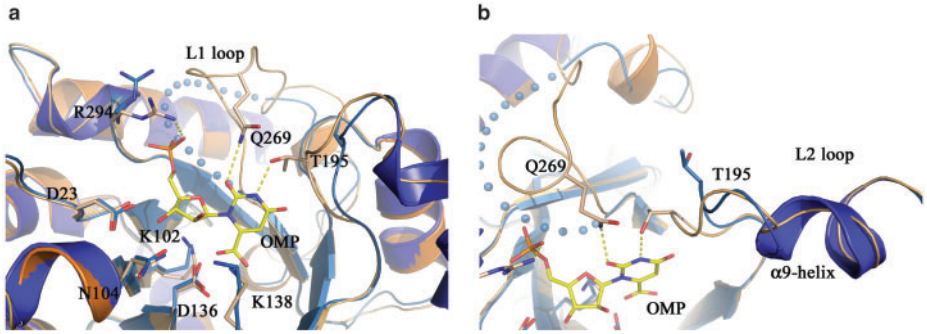

Fig. 3. **Movement of L1 (a) and L2 (b) loops upon bindings of OMP.** Blue and orange structures show the apo form and OMP-complex. (a) The L1 loop, which cannot be unequivocably determined in the apo form (blue dotted line), was stabilized, and the loop structure containing Q269 was formed. (b) The α9 helix only formed in the apo from, and unfolded in association with the movement of Thr195 (C_α distance of 3.8 Å), and then access to the ligand. The figures were drawn with PYMOL (*50*).

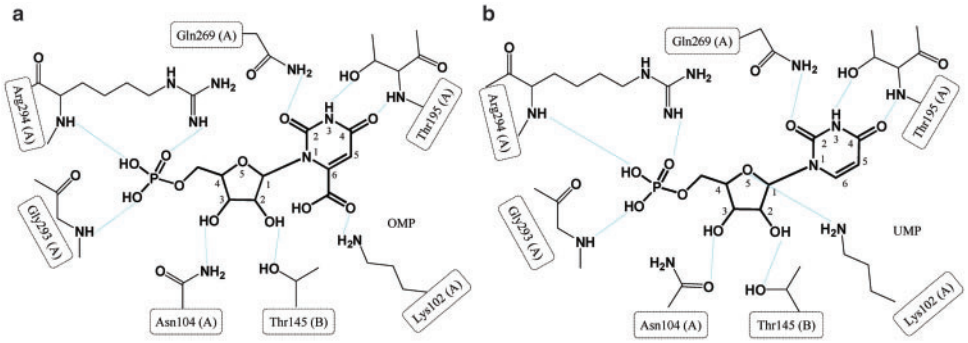

Fig. 4. **Schematic drawings of the hydrogen bonding pattern around OMP (a) and UMP (b).** The binding motif of OMP was basically the same as that of UMP, except for the residue Lys102.

The observed rearrangement of the hydrogen-bond network based on the structural determination of the apo form and OMP- and UMP-complex in *Plasmodium* OMPDCs is the first report.

DISCUSSION

The details of the reaction mechanism have been proposed by Raugei *et al*. (*31*), that a very stable charged network OMP-Lys-Asp-Lys-Asp promotes transition state electrostatic stabilization, and fully conserved Lys138 (*Pf*OMPDC numbering) largely contributes to the stabilization of the transition state or equivalently, the carboanionic intermediate.

In this study, in an attempt to provide further proof-of-principle, we have determined the X-ray structure of the apo, substrate or product-complex forms of *Pf*OMPDC. These three kinds of structural analyses provided an insight into the rearrangement of the hydrogen network in the array of OMP-Lys-Asp-Lys-Asp, by comparison between the initial and completion stages of the decarboxyl reaction. At the initial reaction step, the side chain of Lys102 broke a hydrogen bond with the carboxyl group of Asp136, and then formed a hydrogen bond with the carboxyl oxygen atom of the substrate, upon binding OMP. These processes increased the negative charge on the two carboxyl groups on the substrate and Asp136, which led to electrostatic repulsion between the carboxyl groups. Even the short distance of 2.5 Å between the two carboxyl groups, and the positively charged residues of Lys102 and Lys138 maintained the unstable structure.

Then, the decarboxylation reaction started from the structure with electrostatic repulsion. After direct decarboxylation, the newly generated carboanion at the C6 position of the pyrimidine ring may have been stabilized by the conserved array, and absorbed a proton from the Lys138 side chain directly (*31*). In the completion step, two pairs of hydrogen bonds, Lys102-Asp136 and Lys138-Asp141(B), were formed, and all of the electrostatic charge in the array was compensated (Fig. 5c). It seems to be difficult, however, to specify from our structural models which Lys residues stabilized the forming carboanion intermediate in the transition state.

Ning Wu *et al*. (*47*) reported the mutational study for this enzyme from *M. thermoautotrophicum*. Asp70 and Lys72 (corresponding to Asp136 and Lys138, respectively, in *P. falciparum*) were mutated to an alanine, however those mutants still had enzymatic activity to convert from OMP to UMP, indicating Asp70 cannot be the only driving force for decarboxylation. The same argument can be made for Lys72, and then the mechanism of protonation as well as that of decarboxylation was not specified completely.

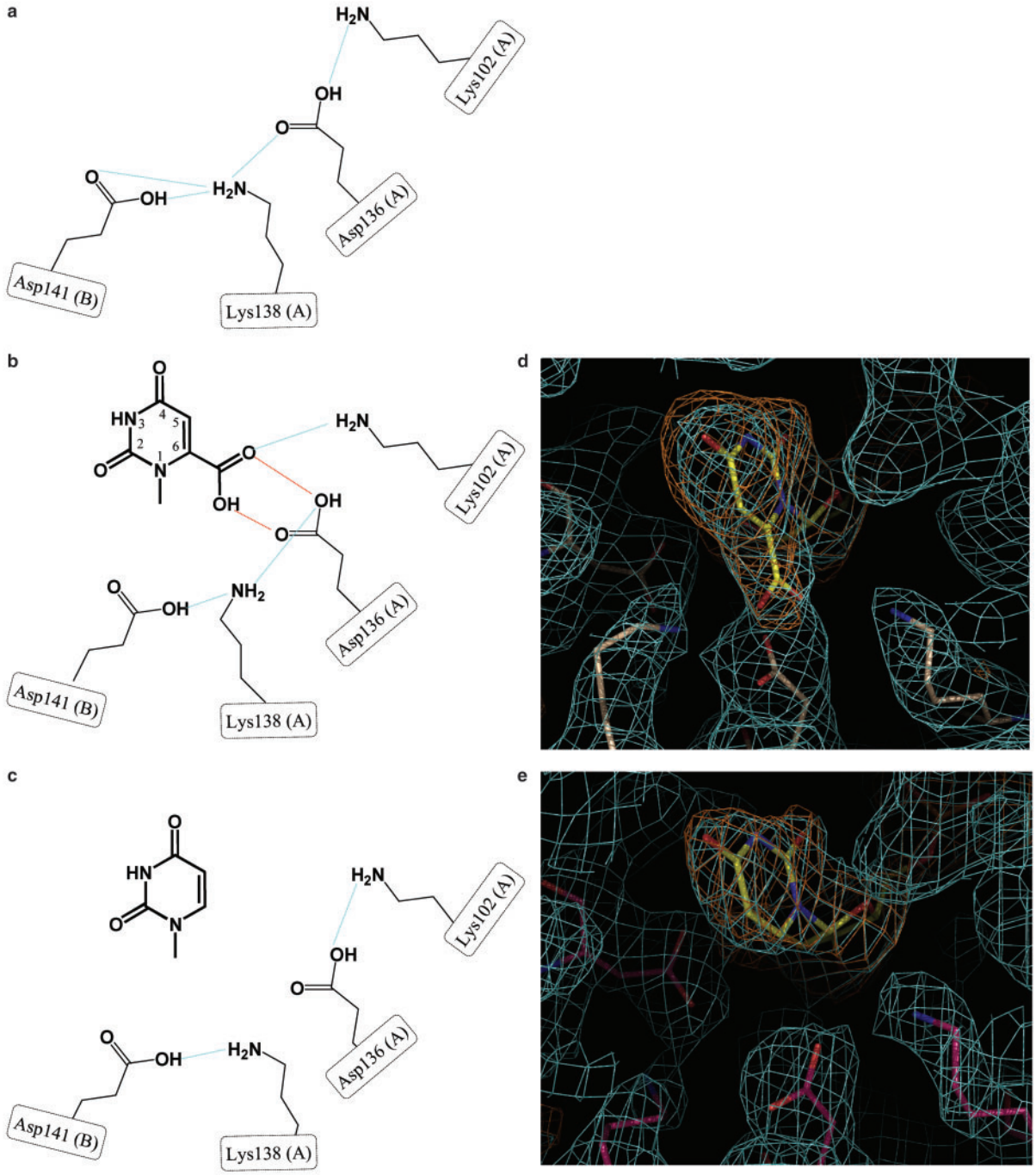

Fig. 5. **Proposed reaction mechanism.** Stepwise representation of the rearrangement of the hydrogen-bond network, with a particular electron density map around Lys102. (a) Apo form. Lys102 formed a hydrogen-bond network with Asp136, Lys138 and Asp141. (b) The substrate entered the active site. As Lys102 turned away from Asp136, charge repulsion between the two carboxylate groups initiated decarboxylation and Lys138 donated a proton to C6. (c) After decarboxylation, Lys102 hydrogen bonded to Asp136 instead of the carboxyl group of the pyrimidine ring. (d) Electron density maps of OMP (d) and UMP (e) binding forms. These contours show the SIGMAA-weighted $2F_o - F_c$ map at 1.5 σ as well as the $F_o - F_c$ omit map. The programs COOT (*46*) and PYMOL (*50*) were used to make these figures.

A structural analysis of complexes with a transition state analogue will further uncover the mechanism of transition state stabilization by Lys residues.

Eukaryotes express OMPDC as a bifunctional protein, UMP synthase, which catalyses the orotate phosphoribosyltransferase reaction before the decarboxylation reaction. On the other hand, *Pf*OMPDC forms a complex with orotate phosphoribosyltransferase (OPRT), which forms a heterotetrameric complex in *P. falciparum* (*20*). In our multiple sequence alignment, we found

a unique structural feature of the OMPDCs belonging to *Plasmodium*. A large insertion was observed between β1 and α5, which formed a protruding domain consisting of three α helices, α2, α3 and α4. We propose that the unique insertion may participate in making a complex with OPRT.

In our structural observations, the top part of the active site played a role in substrate binding, accompanied by large structural movement. The average difference of 1.5 Å in the top part is twice the root-mean-square deviation calculated from all C_α atoms.

Eleven structures of OMPDC have been reported. Among them four kind of nucleotide complex structures are available to compare with those of apo forms to date. Each of OMPDC from *M. thermoautotrophicum, P. horikoshii, E. coli and S. cerevisiae* showed a large structural change around the active site near the open end of the $(\alpha/\beta)_8$ barrel upon binding of the nucleotide. The structure of each loop which corresponds to the L1 loop in *Pf*OMPDC was stabilized by making hydrogen bond with the pyrimidine ring moiety of nucleotide ligands, which is same manner as our complex showed. On the other hand, the OMPDCs from three species except *S. cerevisiae* retained the structure of α-helix which correspond to α9 near the L2 loop region in *Pf*OMPDC, did not display any structural changes upon binding of nucleotide ligands. *Pf*OMPDC has long insertion after α9 helix which makes the L2 loop harder to access to pyrimidine moiety. Therefore α9 helix needs to be unfold upon binding OMP or UMP in *Pf*OMPDC.

On the contrary, the bottom part of the active site was significantly rigid; the average difference was half of the overall root-mean-square deviation. Even a small difference, such as the rearrangement of hydrogen bonds in the array of OMP-Lys-Asp-Lys-Asp, may have played a pivotal role in catalysis. The corresponding residues for binding and catalysing showed >80% consensus among all the OMPDCs, and the structural movements described earlier may be in common with them.

In summary, we have proposed a reaction mechanism and characteristic domain for binding of *Plasmodium* OPRT, as inferred from structural analyses of apo and holo forms. Future studies on the structural analyses of complexes with transition state analogues will unravel the stabilization mechanism of the carboanion intermediate. The structural analysis of the complex between *Pf*OMPDC and *Pf*OPRT will, likewise, clarify the hetero-tetrameric reaction mechanism which could lead to the development of important antimalarial drugs.

The synchrotron radiation experiments were mainly performed at the BL44XU in the SPring-8 with the approval of the Japan Synchrotron Radiation Research Institute (JASRI) (Proposal No. 2006A6806-NL1-np and 2006B6806-NL1-np), and the final data collection was carried out at BL38B1. The authors are grateful to M. Yoshimura, E. Yamashita, A. Nakagawa, M. Kawamoto, N. Shimizu and K. Hasegawa, for their kind support with the data collection at these beam-lines.

This work was supported in part by the program of Grants-in-Aid for Scientific Research (B) (18350086) to T.I., and Founding Research Centers for Emerging and Reemerging Infectious Diseases to TH, of the Ministry of Education, Culture, Sport, Science and Technology (MEXT), Japan, the Thailand Research Fund (BRG 4880006) to S.R.K. and J.K., and a part of a grant from the 21st century Center of Excellence (21COE) Program 'Creation of Integrated EcoChemistry' of Osaka University to K.T.

REFERENCES

1. Guerin, P.J., Olliaro, P., Nosten, F., Druilhe, P., Laxminarayan, R., Binka, F., Kilama, W.L., Ford, N., and White, N.J. (2002) Malaria: current status of control, diagnosis, treatment, and a proposed agenda for research and development. *Lancet Infect. Dis.* **2**, 564–573
2. Ridley, R.G. (2002) Medical need, scientific opportunity and the drive for antimalarial drugs. *Nature* **415**, 686–693
3. Gero, A.M. and O'Sullivan, W.J. (1990) Purines and pyrimidines in malarial parasites. *Blood Cells* **16**, 467–484; discussion 485–498
4. Krungkrai, J., Cerami, A., and Henderson, G.B. (1990) Pyrimidine biosynthesis in parasitic protozoa: purification of a monofunctional dihydroorotase from *Plasmodium berghei and Crithidia fasciculata*. *Biochemistry* **29**, 6270–6275
5. Krungkrai, J., Cerami, A., and Henderson, G.B. (1991) Purification and characterization of dihydroorotate dehydrogenase from the rodent malaria parasite Plasmodium berghei. *Biochemistry* **30**, 1934–1939
6. Umezu, K., Amaya, T., Yoshimoto, A., and Tomita, K. (1971) Purification and properties of orotidine-5′-phosphate pyrophosphorylase and orotidine-5′-phosphate decarboxylase from baker's yeast. *J. Biochem. (Tokyo)* **70**, 249–262
7. Quinn, C.L., Stephenson, B.T., and Switzer, R.L. (1991) Functional organization and nucleotide sequence of the Bacillus subtilis pyrimidine biosynthetic operon. *J. Biol. Chem.* **266**, 9113–9127
8. Jones, M.E. (1980) Pyrimidine nucleotide biosynthesis in animals: genes, enzymes, and regulation of UMP biosynthesis. *Annu. Rev. Biochem.* **49**, 253–279
9. Floyd, E.E. and Jones, M.E. (1985) Isolation and characterization of the orotidine 5′-monophosphate decarboxylase domain of the multifunctional protein uridine 5′-monophosphate synthase. *J. Biol. Chem.* **260**, 9443–9451
10. Livingstone, L.R. and Jones, M.E. (1987) The purification and preliminary characterization of UMP synthase from human placenta. *J. Biol. Chem.* **262**, 15726–15733
11. Yablonski, M.J., Pasek, D.A., Han, B.D., Jones, M.E., and Traut, T.W. (1996) Intrinsic activity and stability of bifunctional human UMP synthase and its two separate catalytic domains, orotate phosphoribosyltransferase and orotidine-5′-phosphate decarboxylase. *J. Biol. Chem.* **271**, 10704–10708
12. Gao, G., Nara, T., Nakajima-Shimada, J., and Aoki, T. (1999) Novel organization and sequences of five genes encoding all six enzymes for de novo pyrimidine biosynthesis in Trypanosoma cruzi. *J. Mol. Biol.* **285**, 149–161
13. Nara, T., Hshimoto, T., and Aoki, T. (2000) Evolutionary implications of the mosaic pyrimidine-biosynthetic pathway in eukaryotes. *Gene* **257**, 209–222
14. Weber, G. (1983) Biochemical strategy of cancer cells and the design of chemotherapy: G. H. A. Clowes Memorial Lecture. *Cancer Res.* **43**, 3466–3492
15. Scott, H.V., Gero, A.M., and O'Sullivan, W.J. (1986) In vitro inhibition of Plasmodium falciparum by pyrazofurin, an inhibitor of pyrimidine biosynthesis de novo. *Mol. Biochem. Parasitol.* **18**, 3–15

16. Queen, S.A., Jagt, D.L., and Reyes, P. (1990) In vitro susceptibilities of Plasmodium falciparum to compounds which inhibit nucleotide metabolism. *Antimicrob. Agents Chemother.* **34**, 1393–1398
17. Krungkrai, J., Krungkrai, S.R., and Phakanont, K. (1992) Antimalarial activity of orotate analogs that inhibit dihydroorotase and dihydroorotate dehydrogenase. *Biochem. Pharmacol.* **43**, 1295–1301
18. Seymour, K.K., Lyons, S.D., Phillips, L., Rieckmann, K.H., and Christopherson, R.I. (1994) Cytotoxic effects of inhibitors of de novo pyrimidine biosynthesis upon *Plasmodium falciparum*. *Biochemistry* **33**, 5268–5274
19. Miller, B.G., Snider, M.J., Wolfenden, R., and Short, S.A. (2001) Dissecting a charged network at the active site of orotidine-5′-phosphate decarboxylase. *J. Biol. Chem.* **276**, 15174–15176
20. Krungkrai, S.R., DelFraino, B.J., Smiley, J.A., Prapunwattana, P., Mitamura, T., Horii, T., and Krungkrai, J. (2005) A novel enzyme complex of orotate phosphoribosyltransferase and orotidine 5′-monophosphate decarboxylase in human malaria parasite *Plasmodium falciparum*: physical association, kinetics, and inhibition characterization. *Biochemistry* **44**, 1643–1652
21. Miller, B.G. and Wolfenden, R. (2002) Catalytic proficiency: the unusual case of OMP decarboxylase. *Annu. Rev. Biochem.* **71**, 847–885
22. Wu, N., Mo, Y., Gao, J., and Pai, E.F. (2000) Electrostatic stress in catalysis: structure and mechanism of the enzyme orotidine monophosphate decarboxylase. *Proc. Natl Acad. Sci. USA* **97**, 2017–2022
23. Harris, P., Navarro Poulsen, J.C., Jensen, K.F., and Larsen, S. (2000) Structural basis for the catalytic mechanism of a proficient enzyme: orotidine 5′-monophosphate decarboxylase. *Biochemistry* **39**, 4217–4224
24. Appleby, T.C., Kinsland, C., Begley, T.P., and Ealick, S.E. (2000) The crystal structure and mechanism of orotidine 5′-monophosphate decarboxylase. *Proc. Natl. Acad. Sci. USA* **97**, 2005–2010
25. Feng, W.Y., Austin, T.J., Chew, F., Gronert, S., and Wu, W. (2000) The mechanism of orotidine 5′-monophosphate decarboxylase: catalysis by destabilization of the substrate. *Biochemistry* **39**, 1778–1783
26. Houk, K.N., Lee, J.K., Tantillo, D.J., Bahmanyar, S., and Hietbrink, B.N. (2001) Crystal structures of orotidine monophosphate decarboxylase: does the structure reveal the mechanism of nature's most proficient enzyme? *Chembiochem* **2**, 113–118
27. Begley, T.P., Appleby, T.C., and Ealick, S.E. (2000) The structural basis for the remarkable catalytic proficiency of orotidine 5′-monophosphate decarboxylase. *Curr. Opin. Struct. Biol.* **10**, 711–718
28. Wu, N. (2002) Crystal structures of inhibitor complexes reveal an alternate binding mode in orotidine-5′-monophosphate decarboxylase. *J. Biol. Chem.* **277**, 28080–28087
29. Warshel, A., Strajbl, M., Villa, J., and Florian, J. (2000) Remarkable rate enhancement of orotidine 5′-monophosphate decarboxylase is due to transition-state stabilization rather than to ground-state destabilization. *Biochemistry* **39**, 14728–14738
30. Hur, S. and Bruice, T.C. (2002) Molecular dynamic study of orotidine-5′-monophosphate decarboxylase in ground state and in intermediate state: a role of the 203-218 loop dynamics. *Proc. Natl. Acad. Sci. USA* **99**, 9668–9673
31. Raugei, S., Cascella, M., and Carloni, P. (2004) A proficient enzyme: insights on the mechanism of orotidine monophosphate decarboxylase from computer simulations. *J. Am. Chem. Soc.* **126**, 15730–15737
32. Miller, B.G., Hassell, A.M., Wolfenden, R., Milburn, M.V., and Short, S.A. (2000) Anatomy of a proficient enzyme: the structure of orotidine 5′-monophosphate decarboxylase in the presence and absence of a potential transition state analog. *Proc. Natl. Acad. Sci. USA* **97**, 2011–2016
33. Miller, B.G., Snider, M.J., Short, S.A., and Wolfenden, R. (2000) Contribution of enzyme-phosphoribosyl contacts to catalysis by orotidine 5′-phosphate decarboxylase. *Biochemistry* **39**, 8113–8118
34. Porter, D.J. and Short, S.A. (2000) Yeast orotidine-5′-phosphate decarboxylase: steady-state and pre-steady-state analysis of the kinetic mechanism of substrate decarboxylation. *Biochemistry* **39**, 11788–11800
35. Smiley, J.A. and Jones, M.E. (1992) A unique catalytic and inhibitor-binding role for Lys93 of yeast orotidylate decarboxylase. *Biochemistry* **31**, 12162–12168
36. Lee, J.K. and Houk, K.N. (1997) A proficient enzyme revisited: the predicted mechanism for orotidine monophosphate decarboxylase. *Science* **276**, 942–945
37. Phillips, L.M. and Lee, J.K. (2001) Theoretical studies of mechanisms and kinetic isotope effects on the decarboxylation of orotic acid and derivatives. *J. Am. Chem. Soc.* **123**, 12067–12073
38. Laemmli, U.K. (1970) Cleavage of structural proteins during the assembly of the head of bacteriophage T4. *Nature* **227**, 680–685
39. Krungkrai, S.R., Tokuoka, K., Kusakari, Y., Inoue, T., Adachi, H., Matsumura, H., Takano, K., Murakami, S., Mori, Y., Kai, Y., Krungkrai, J., and Horii, T. (2006) Crystallization and preliminary crystallographic analysis of orotidine 5′-monophosphate decarboxylase from the human malaria parasite Plasmodium falciparum. *Acta. Crystallograph. Sect. F. Struct. Biol. Cryst. Commun.* **62**, 542–545
40. MOSFLM. (Data-collection) Leslie, A.G.W. (1992) *Joint CCP4 and ESF-EACMB Newsletter on Protein Crystallography* Vol. 26, Daresbury Laboratory, Warrington, UK
41. Otwinowski, Z. and Minor, W. (1997) Processing of X-ray diffraction data collected in oscillation mode. *Methods Enzymol.* **276**, 307–326
42. Navaza, J. (2001) Implementation of molecular replacement in AMoRe. *Acta. Crystallogr. D. Biol. Crystallogr.* **57**, 1367–1372
43. Collaborative Computational Project, n. (1994) The CCP4 suite: programs for protein crystallography. *Acta Crystallogr. D. Biol. Crystallogr.* **50**, 760–763. Write to the Help Desk NCBI | NLM | NIH Department of Health & Human Services Privacy Statement | Freedom of Information Act | Disclaimer
44. Brunger, A.T., Adams, P.D., Clore, G.M., DeLano, W.L., Gros, P., Grosse-Kunstleve, R.W., Jiang, J.S., Kuszewski, J., Nilges, M., Pannu, N.S., Read, R.J., Rice, L.M., Simonson, T., and Warren, G.L. (1998) Crystallography and NMR system: a new software suite for macromolecular structure determination. *Acta Crystallogr. D. Biol. Crystallogr.* **54**, 905–921
45. Murshudov, G.N., Vagin, A.A., Lebedev, A., Wilson, K.S., and Dodson, E.J. (1999) Efficient anisotropic refinement of macromolecular structures using FFT. *Acta Crystallogr. D. Biol. Crystallogr.* **55**, 247–255
46. Emsley, P. and Cowtan, K. (2004) Coot: model-building tools for molecular graphics. *Acta Crystallogr. D. Biol. Crystallogr.* **60**, 2126–2132
47. Wu, N., Gillon, W., and Pai, E.F. (2002) Mapping the active site-ligand interactions of orotidine 5′-monophosphate decarboxylase by crystallography. *Biochemistry* **41**, 4002–4011

48. Vedadi, M., Lew, J., Artz, J., Amani, M., Zhao, Y., Dong, A., Wasney, G.A., Gao, M., Hills, T., Brokx, S., Qiu, W., Sharma, S., Diassiti, A., Alam, Z., Melone, M., Mulichak, A., Wernimont, A., Bray, J., Loppnau, P., Plotnikova, O., Newberry, K., Sundararajan, E., Houston, S., Walker, J., Tempel, W., Bochkarev, A., Kozieradzki, I., Edwards, A., Arrowsmith, C., Roos, D., Kain, K., and Hui, R. (2007) Genome-scale protein expression and structural biology of Plasmodium falciparum and related Apicomplexan organisms. *Mol. Biochem. Parasitol.* **151**, 100–110
49. Harris, P., Poulsen, J.C., Jensen, K.F., and Larsen, S. (2002) Substrate binding induces domain movements in orotidine 5′-monophosphate decarboxylase. *J. Mol. Biol.* **318**, 1019–1029
50. DeLano, W.L. (2005) The case for open-source software in drug discovery. *Drug Discov. Today* **10**, 213–217